Energy-efficient predictive control of indoor thermal comfort and air quality in a direct expansion air conditioning system

Jun Mei, Xiaohua Xia

Centre of New Energy Systems, Department of Electrical, Electronic and Computer Engineering, University of Pretoria, Pretoria 0028, South Africa

Abstract

Generally, conventional controllers for comfort are designed by using on/off control or proportional-integral (PI) control, with little consideration of energy consumption of the system. This paper presents a multi-input-multi-output (MIMO) model predictive control (MPC) for a direct expansion (DX) air conditioning (A/C) system to improve both indoor thermal comfort and air quality, whereas the energy consumption is minimised. The DX A/C system is modelled into a nonlinear system, with a varying speed of compressor and varying speed of supply fan and volume flow rate of supply air being regarded as inputs. We first propose an open loop controller based on an optimisation of energy consumption with the advantage of a unique set of steady states. The MPC controller is proposed to optimise the transient processes reaching the steady state. To facilitate the MPC design, the nonlinear model is linearised around its steady state. MPC is designed for the linearised model. The advantages of the proposed energy-optimised open loop controller and the closed-loop regulation of the MIMO MPC scheme are verified by simulation results.

Keywords: Temperature and humidity; model predictive control; CO_2 concentration; open loop optimisation; energy efficiency; DX A/C system

Nomenclature	
A_1	heat transfer area of the DX evaporator in the dry-cooling region, m^2
A_2	heat transfer area of the DX evaporator in the wet-cooling region, m^2
C_a	specific heat of air, kJ kg^{-1} °C^{-1}
V_f	air volumetric flow rate, m^3/s
$M_{h,load}$	moisture load in the conditioned space, kg/s
M_{rmf}	mass flow rate of refrigerant, kg/s
Q_{load}	sensible heat load in the conditioned space, kW
T_e	temperature of air leaving the DX evaporator, °C
T_{cs}	air temperature in the conditioned space, °C
T_d	air temperature leaving the dry-cooling region on air side, °C
T_w	temperature of the DX evaporator wall, °C
V	volume of the conditioned space, m^3
V_{com}	swept volume of the rotor compressor, m^3
W_e	moisture content of air leaving the DX evaporator, kg/kg dry air
W_{cs}	moisture content of air-conditioned space, kg/kg dry air
α_1	heat transfer coefficient between air and the DX evaporator wall in the dry-cooling region, kW m^{-2} °C^{-1}
α_2	heat transfer coefficient between air and the DX evaporator wall in the wet-cooling region, kW m^{-2} °C^{-1}
ρ	density of moist air, kg/m^3
h_{fg}	latent heat of vaporisation of water, kJ/kg
h_{r1}	enthalpy of refrigerant at vaporisation inlet, kJ/kg
h_{r2}	enthalpy of refrigerant at vaporisation outlet, kJ/kg
k_{spl}	coefficient of supply fan heat gain, kJ/m^3
v_s	specific volume of superheated refrigerant, m^3/kg
V_{sc}	speed of compressor, rpm
k_{fan}	coefficient of supply fan speed, m^3/r
V_{h1}	air side volume of the DX evaporator in the dry-cooling region on air side, m^3
V_{h2}	air side volume of the DX evaporator in the wet-cooling region on air side, m^3
λ	compressor's displacement coefficient
BESTEST	building energy simulation test
ASHRAE	American Society of Heating, Refrigerating, and Air-Conditioning Engineers

1. Introduction

Nowadays, approximately $30 - 40\%$ of all primary energy in the world is consumed by the building sector, where a significant portion is used to improve

indoor air quality and thermal comfort, accounting for a large amount of greenhouse gas emissions. When energy is overused, it would result in a shortage of energy. Meanwhile, the global temperature has steadily increased due to greenhouse effects, which in turn makes the use of air conditioning grow. Therefore, reducing the energy consumption in buildings is a key factor in reducing national greenhouse gas emissions. Energy management of building air conditioning systems becomes fundamentally necessary to improve the energy efficiency and reduce the energy cost of buildings. Energy efficiency improvement of buildings can also be made through other means of interventions [1, 2] such as hybrid energy supplies [3]-[9], appliances operation scheduling [10]-[15], facility retrofitting and maintenance [16]-[21], envelope retrofitting [22], lighting retrofitting [23, 24] and energy-water nexus [25, 26].

Reducing energy consumption does not necessarily sacrifice user welfare or equipment performance [27]; in some aspects, user health is in accordance with energy efficiency. For example, more and more people are spending a substantial amount of time indoors, therefore improving thermal comfort and indoor air quality for the occupants would contribute to productivity and efficiency. In buildings, controlling indoor humidity at an appropriate level is crucial since this directly affects building occupants' thermal comfort and the operating efficiency of building air conditioning installations [28]. Various humidity control strategies applied to large-scale central air conditioning (A/C) systems, such as heat pipe technology and pre-conditioning outdoor air [29, 30], or chemical dehumidification desiccant mechanisms [31, 32] and mechanical dehumidification desiccant mechanisms [33, 34] are not applicable to direct expansion (DX) A/C systems. Compared to central chilled water-based A/C systems, DX A/C systems are simpler in system configuration, more energy efficient [35] and cost less to own and maintain. Therefore, DX A/C systems have been widely used over recent decades in buildings, especially in small to medium scaled buildings. However, most DX A/C systems currently are equipped with single-speed compressors and supply fans by on/off cycling compressors as a low-cost approach only to maintain indoor air temperature, and this leads to either space overcooling or uncontrolled equilibrium indoor air humidity. Therefore, on/off cycling leads to a degraded level of thermal comfort for occupants. With the advancement of variable speed drive technology, it becomes possible for DX A/C systems with the varying speeds of compressors and supply fans to achieve simultaneous control of indoor air temperature and humidity [36].

Various control strategies designed and employed for DX A/C systems are to control indoor air temperature and humidity simultaneously. An experimental investigation indicated that a conventional PID control method proposed to maintain indoor air temperature by varying compressor speed, and indoor air humidity by varying supply fan speed, separately, may be controlled simultaneously [37]. Since the strong cross-coupling between two decoupled feedback loops (i.e., the control loop for temperature by varying compressor speed and that for humidity by varying supply fan speed), the transient performance of the two feedback loops was inherently inferior. Consequently, this control strategy remained inadequate.

3

To overcome the difficulties of the coupling effect, more advanced control strategies have been reported. A novel direct digital (DDC)-based capacity controller for a variable speed DX A/C system to control indoor air temperature and humidity simultaneously has been developed in [38, 39]. In [40], Qi and Deng presents a multivariable dynamic model of the variable speed DX A/C system taking into account the coupling effects among multiple variables. The state-space representation was linearised at a particular operational point, to facilitate developing a multi-input multi-output (MIMO) controller which is capable of addressing couplings and is more effective in simultaneously achieving multiple control objectives, such as temperature, humidity, capacity and efficiency. The model was experimentally validated. Besides, Qi and Deng [41] proposed MIMO Linear Quadratic Gaussian (LQG) control strategy for simultaneously controlling indoor air temperature and humidity by regulating the varying speeds of the compressor and supply fan in an experimental DX A/C system. The MIMO controller developed can effectively control indoor air temperature and humidity simultaneously, with command following and disturbance rejection capability tests. However, these papers did not discuss indoor CO_2 concentration control. In [42], an artificial neural network (ANN)-based controller is proposed for a variable speed DX A/C system to control indoor air temperature and humidity simultaneously. In [43], a novel hybrid steady-state model based controller (SSMBC) is proposed to control indoor air temperature and humidity simultaneously. The experiment shows that the novel hybrid SSMBC is accurate and sensitive. In [44], a novel Proportional-Derivative (PD) law based fuzzy logic controller for a variable speed DX A/C system is designed to control indoor air temperature and humidity simultaneously.

In recent years, indoor air quality is more and more regulated by A/C system design and control. The CO_2 concentration, air temperature and humidity have become three major indicators of indoor comfort and air quality. In [45, 46], Zhu et. al., studied indoor air temperature, humidity and CO_2 concentration control simultaneously, but without consideration the coupling effect. Three coupling effects cannot be ignored in many cases. In fact, the experimental investigation [47] suggested that the indoor CO_2 concentration affected indoor air temperature. Furthermore, indoor humidity was correlated with CO_2 concentration according to measurement results reported in [48]. To our best knowledge, very little work exists in the literature to study indoor air temperature, humidity and CO_2 concentration control simultaneously with consideration of coupling effects and energy efficiency. This paper studies the optimisation of DX A/C systems that strikes a balance of indoor comfort, air quality as well as energy efficiency.

Nonlinear control systems for indoor air temperature, humidity and CO_2 concentration in DX A/C system have been modelled with considering the coupling effects of indoor air temperature, humidity and CO_2 concentration. The energy consumption model for the DX A/C system is given. The open loop optimal method is used to optimise the energy consumption model for the DX A/C system, such that there would be a unique and optimal steady state for the closed-loop system to follow. The nonlinear control system can be linearised

4

around the steady state. An advanced model predictive control (MPC) strategy is proposed to regulate the indoor air temperature, humidity and CO_2 concentration along the steady state. The energy consumption for different temperature, humidity and CO_2 concentration reference following are developed. The simulation results show that, with the optimal steady state obtained from open loop optimisation, the integrated scheme could improve not only the temperature, humidity and CO_2 concentration level but also energy efficiency in the DX A/C system. Besides, disturbances due to other indoor factors can be addressed. The main contributions of this paper include four main areas. Firstly, a nonlinear model is proposed for the study of the indoor comfort in terms of air temperature and humidity, and indoor air quality in terms of CO_2 concentration, of a DX A/C system, by taking into consideration of the coupling effects. Secondly, the open loop method on energy efficiency is adopted for finding the unique steady state of the DX A/C system. Thirdly, the indoor air temperature, humidity and CO_2 concentration are maintained simultaneously by using the proposed MPC approach in the circumstance of disturbances. Finally, with the proposed control, the indoor temperature, humidity and CO_2 concentration are optimised for superior energy efficiency. This paper introduces two economical and advanced energy-based optimised open loop controller and the closed-loop regulation of the MPC method that not only maintains indoor thermal comfort and air quality but also minimizes the amount of energy consumed.

The paper is organised as follows. The DX A/C system is described and modelled in Section 2. An open loop optimal controller is proposed by optimising the energy consumption model to obtain the unique steady state, around which the nonlinear model of DX A/C system is linearised in Section 3. The discrete-time system, the objective function for regulating the indoor air temperature, humidity and CO_2 concentration and constraints for states and inputs are presented for the closed-loop MPC controller in Section 4. The results of the MIMO MPC for maintaining the indoor air temperature, humidity and CO_2 concentration are reported in Section 5.

2. System description

2.1. DX A/C system

A simplified schematic diagram of the system is shown in Fig. 1. The DX A/C system is mainly composed of two parts, namely, a DX refrigeration plant (refrigerant side) and air-distribution sub-system (air side). The major components of the DX refrigeration plant consist of five parts: a variable speed rotor compressor, an electronic expansion valve (EEV), a high-efficiency tube-louver-finned DX evaporator, a variable air volume (VAV) and an air-cooled tube-plant-finned condenser. The evaporator is placed inside the supply air duct to work as a DX air cooling coil. The air-distribution sub-system includes an air-distribution ductwork with return air dampers, a variable speed centrifugal supply fan and a conditioned thermal space.
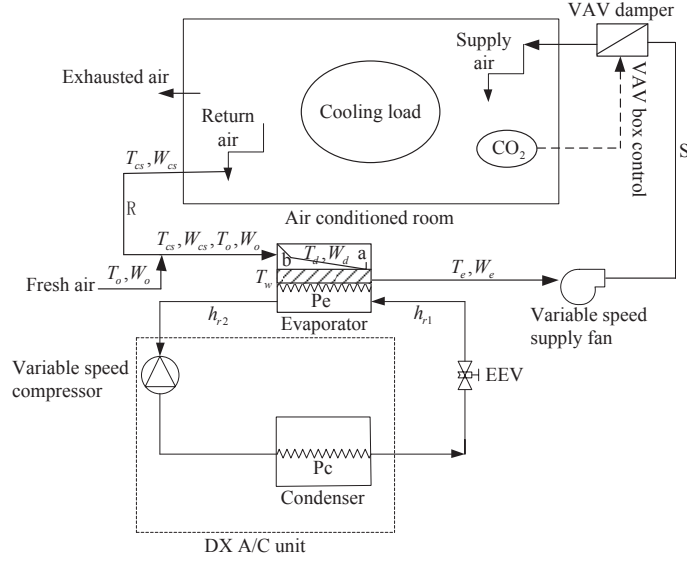
Figure 1: Simplified schematic diagram of the DX A/C system.

2.2. Air conditioning room

In this paper, a single-zone building model (that has been used in the building energy simulation test (BESTEST) [49]) is applied to evaluate the performance of proposed MPC strategy. The structure of the single-zone building model is displayed in Fig. 2.

2.3. System dynamic model

The dynamical model of the DX A/C system based on energy and mass conservation principles is highly nonlinear with respect to temperature, moisture content and CO_2 concentration. In this paper, the system is considered to operate in the cooling mode. The basic operation and assumptions of the system in the cooling mode are given as follows. These assumptions are standard in the literature [41] and are sometimes made for simplistic purposes.

(A1) A percentage (denoted by p, $0 < p < 1$) of fresh air is allowed into the system and gets mixed with $1 - p$ of the recirculated air at the evaporator.

(A2) Sufficient air mixing occurs inside the heat exchangers where it gets conditioned.

(A3) The air side of the DX evaporator can be divided into two regions, i.e., the dry-cooling region and wet-cooling region; the air temperature decreases in the dry-cooling region and the dehumidification mainly takes place in the wet-cooling region; the evaporator diagram is shown in Fig. 1; the dry region b is generally very small and used to keep the decreased temperature, and the wet-region a is used to couple air cooling and dehumidification.

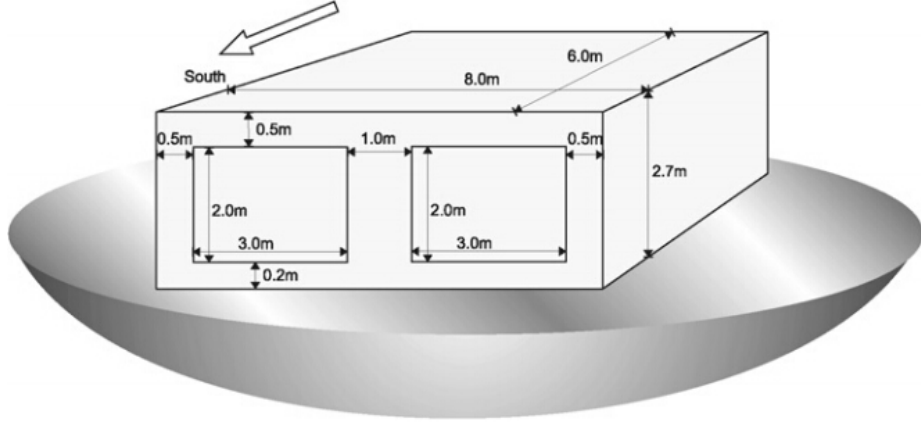(A4) Thermal losses in air ducts are negligible.

6

Figure 2: Building model.

(A5) The supply air enters the air-conditioned room to offset the cooling loads acting upon the system.

(A6) The air in the conditioned room is drawn through a fan, $1 - p$ of this air gets recirculated and the rest is exhausted from the system by a fan.

(A7) The heat transfer coefficients of DX A/C system are constant values.

In the DX A/C system, T_e and W_e are the temperature and moisture contents of the air leaving the DX cooling coil respectively, as shown in Fig. 1. Supposing perfect air mixing, air temperature T_{cs} and moisture content W_{cs} leaving the conditioned space can be regarded as being equal to these in the conditioned thermal space. Based on the above assumptions, the energy and mass conservation equations of DX A/C system can be written as follows.

The dynamic mathematical equation of the energy balance for the temperature of conditioned space is given by:

$$C_a \rho V \frac{\mathrm{d}T_{cs}}{\mathrm{d}t} = C_a \rho V_f (T_e - T_{cs}) + Q_{load} + Q_{spl}, \tag{1}$$

where V is the volume of the conditioned space; ρ is the air mass density; C_a is the specific heat of air. V_f is the air volumetric flow rate, which is described by the following:

$$V_f = k_{fan} S_{fan},$$

where k_{fan} is the coefficient of supply fan speed, and S_{fan} is the supply fan speed. Space sensible heat load Q_{load}, which refers to the dry bulb temperature of the building, is usually related to occupants and electrical devices. The heat emitted from electrical devices is easy to identify based on the electrical characteristics of the devices; the main uncertainty in identifying the sensible loads are due to the load associated to occupants, which can be modelled using the current CO_2 concentration in the conditioning room. Therefore, the sensible heat load can be modelled by the following equation

$$Q_{load} = \mu C_c + \nu, \tag{2}$$

7

where C_c represents the CO$_2$ concentration in the room (ppm). μ and ν are the sensible heat gain parameters. The heat gain Q_{spl} of supply fan increased with the air volumetric flow rate as follows:

$$Q_{spl} = k_{spl}V_f, \tag{3}$$

where k_{spl} is the coefficient of supply fan heat gain.

The dynamic mathematical equation of energy conservation of the moisture content inside the conditioned space can be expressed as:

$$\rho V h_{fg}\frac{\mathrm{d}W_{cs}}{\mathrm{d}t} = \rho h_{fg}V_f(W_e - W_{cs}) + M_{h,load}, \tag{4}$$

where h_{fg} represents the latent heat of vaporisation of water. The latent heat loads $M_{h,load}$, which refer to the wet bulb temperature of the building, are related to occupants and electrical devices. Therefore, the latent heat loads can be modelled by the following equation

$$M_{h,load} = \phi C_c + \gamma, \tag{5}$$

where ϕ and γ are the moisture heat gain parameters.

The energy balance principle in the dry-cooling region on the air side is given as:

$$C_a\rho V_{h1}\frac{\mathrm{d}T_d}{\mathrm{d}t} = C_a\rho V_f(T_{cs} - T_d) + \alpha_1 A_1(T_w - \frac{(1-p)T_{cs} + pT_0 + T_d}{2}), \tag{6}$$

where V_{h1} is the air side volume of the DX evaporator in the dry-cooling region, T_d denotes the air temperature leaving the dry-cooling region of the DX evaporator. T_w is the temperature of the DX evaporator wall, A_1 is the heat transfer area of the DX evaporator in the dry-cooling region, and α_1 is the heat transfer coefficient; T_o is the temperature of the outdoor air.

Due to the strong coupling between temperature and moisture content, the energy balance in the wet-cooling region can be written in an enthalpy form [40]:

$$\begin{aligned} C_a\rho V_{h2}\frac{\mathrm{d}T_e}{\mathrm{d}t} + \rho V_{h2}h_{fg}\frac{\mathrm{d}W_e}{\mathrm{d}t} = &C_a\rho V_f(T_d - T_e) + \rho V_f h_{fg}((1-p)W_{cs} + \\ &pW_0 - W_e) + \alpha_2 A_2(T_w - \frac{T_d + T_e}{2}), \end{aligned} \tag{7}$$

where V_{h2} is the air side volume of the DX evaporator in the wet-cooling region, α_2 is the heat transfer coefficient. A_2 is the heat transfer area of the DX evaporator in the wet-cooling region, W_o is the moisture content of the outdoor air.

The dynamic mathematical equation of the energy balance for the evaporator wall is given by:

$$\begin{aligned} C_{a,w}\rho_w V_w\frac{\mathrm{d}T_w}{\mathrm{d}t} = &\alpha_1 A_1(\frac{(1-p)T_{cs} + pT_0 + T_d}{2} - T_w) + \alpha_2 A_2(\frac{T_d + T_e}{2} \\ &- T_w) - M_{rmf}(h_{r2} - h_{r1}), \end{aligned} \tag{8}$$

and the refrigerant mass flow rate M_{rmf} can be determined by [41]:

$$M_{rmf} = \frac{V_{sc}V_{com}}{v_s}\lambda = \frac{V_{sc}V_{com}}{v_s}(1 - 0.015[(P_c/P_e)^{1/\beta}]),$$

where $C_{a,w}$, ρ_w and V_w mean the specific heat of air in the evaporator wall, the density of the evaporator wall and the volume of the evaporator wall, respectively. V_{sc} is the speed of the compressor, λ is the compressor displacement coefficient. V_{com} is the swept volume of the rotor compressor, v_s is the specific volume of superheated refrigerant, β is the compressor index which is assumed to be constant at 1.18. h_{r1} and h_{r2} are the enthalpies of refrigerants at evaporator inlet and outlet, respectively. P_c and P_e are the condensing pressure and the evaporating pressure, respectively.

The supply air leaving the DX evaporator is assumed to be approximately 95% saturated. The relationship between air moisture content and temperature can be derived by plotting and curving fitting [41]:

$$\frac{\mathrm{d}W_e}{\mathrm{d}t} - \frac{2 \times 0.0198T_e + 0.085}{1000}\frac{\mathrm{d}T_e}{\mathrm{d}t} = 0. \tag{9}$$

The dynamic model of indoor CO_2 concentration can be described by the following differential equation [50]:

$$V\frac{\mathrm{d}C_c}{\mathrm{d}t} = V_c(C_0 - C_c) + GP, \tag{10}$$

where V_c represents the volume flow rate of supply air; C_0 denotes the CO_2 concentration of supply air; G is the amount of CO_2 emission rate of people; P is the number of occupants.

The proposed DX A/C system is described by nonlinear equations of (1)-(10), which can be written compactly as follows:

$$\dot{x} = f(x, u) = D^{-1}f_1(x, u) + D^{-1}f_2(z), \tag{11}$$

where $x \triangleq [T_e\ T_{cs}\ T_d\ T_w\ W_e\ W_{cs}\ C_c]^T$, $u \triangleq [V_f\ M_{rmf}\ V_c]^T$, and $z \triangleq [\nu\ \gamma\ GP]^T$, f_1, f_2 are the functions defined as follows:

$$\begin{aligned}
f_1(x, u) =& [f_{11}\ f_{12}\ f_{13}\ f_{14}\ f_{15}\ 0\ f_{17}]^T, \\
f_{11} =& C_a\rho V_f(T_e - T_{cs}) + \mu C_c + k_{spl}V_f, \\
f_{12} =& \rho h_{fg}V_f(W_e - W_{cs}) + \phi C_c, \\
f_{13} =& C_a\rho V_f(T_{cs} - T_d) + \alpha_1 A_1(T_w - \frac{(1-p)T_{cs} + pT_0 + T_d}{2}), \\
f_{14} =& C_a\rho V_f(T_d - T_e) + \rho V_f h_{fg}((1-p)W_{cs} + pW_0 - W_e) + \alpha_2 A_2(T_w - \\
& \frac{T_d + T_e}{2}), \\
f_{15} =& \alpha_1 A_1(\frac{T_d + (1-p)T_{cs} + pT_0}{2} - T_w) + \alpha_2 A_2(\frac{T_d + T_e}{2} - T_w) - \\
& M_{rmf}(h_{r2} - h_{r1}), \\
f_{17} =& V_c(C_0 - C_c),
\end{aligned}$$

9

$$f_2(z) = \begin{bmatrix} \mu & \nu & 0 & 0 & 0 & 0 & GP \end{bmatrix}^T;$$

and the coupling matrix D is given by

$$D = \begin{bmatrix} 0 & C_a\rho V & 0 & 0 & 0 & 0 & 0 \\ 0 & 0 & 0 & 0 & 0 & \rho V h_{fg} & 0 \\ 0 & 0 & C_a\rho V_{h1} & 0 & 0 & 0 & 0 \\ C_a\rho V_{h2} & 0 & 0 & 0 & \rho V_{h2}h_{fg} & 0 & 0 \\ 0 & 0 & 0 & C_{a,w}\rho_w V_w & 0 & 0 & 0 \\ -\frac{2\times 0.0198T_e + 0.085}{1000} & 0 & 0 & 0 & 1 & 0 & 0 \\ 0 & 0 & 0 & 0 & 0 & 0 & V \end{bmatrix}.$$

The system models (1), (4), (6)-(9) were validated in [40] by experimental data. The model (10) was verified in [50] with an on-line learning and estimation approach for model parameter identification with acceptable accuracy.

3. Open loop optimisation

3.1. Open loop controller

An open loop controller is designed to steer the system to operate around its reference temperature, humidity and CO_2 concentration. The energy consumption model is given as an optimising objective.

The energy consumption of DX A/C system includes the input power of the evaporator $P_{eva,fan}$, the input power of the compressor P_{comp}, the input power of the condenser $P_{con,fan}$ and the input power of the ventilation fan P_{ven}. Therefore, the DX A/C energy consumption is expressed in (12):

$$P_{total} = P_{eva,fan} + P_{con,fan} + P_{comp} + P_{ven}, \tag{12}$$

where P_{total} is the energy consumption of the DX A/C system.

The input power of the evaporator fan $P_{eva,fan}$ can be expressed as a function of the air volumetric flow rate, building cooling load and supply air temperature as follows [51]:

$$\begin{aligned} P_{eva,fan} =& a_0 + a_1 V_f + a_2 V_f^2 + a_3 T_e + a_4 T_e^2 + a_5 Q_{cool} + a_6 Q_{cool}^2 \\ &+ a_7 V_f T_e + a_8 V_f Q_{cool} + a_9 T_e Q_{cool}, \end{aligned} \tag{13}$$

where coefficients a_i ($i = 0, 1, \ldots, 9$) are constant, which can be determined by curve-fitting of experimental data. The building cooling load Q_{cool} is the summation of sensible heat loads and moisture heat loads.

The empirical expression to determine the power consumption of the compressor P_{comp} is proposed as follows [52]:

$$\begin{aligned} P_{comp} =& b_0 + b_1 T_d + b_2 T_e + b_3 T_d^2 + b_4 T_d T_e + b_5 T_e^2 + \\ & b_6 T_d^3 + b_7 T_d^2 T_e + b_8 T_d T_e^2 + b_9 T_e^3, \end{aligned} \tag{14}$$

where coefficients b_i $(i = 0, 1, \ldots, 9)$ are constant, which can be determined by curve-fitting of the experimental data. Note that in [51, 52], it was shown that polynomials fit better with experimental data.

The power consumption of the condenser $P_{con,fan}$ is [51]:

$$P_{con,fan} = c_0 + c_1 M_{rmf} + c_2 M_{rmf}^2, \tag{15}$$

where coefficients c_i $(i = 0, 1, 2)$ are constant to be determined by curve-fitting of the experimental data.

The energy consumption of the ventilation fan for controlling indoor CO_2 concentration can be modelled to be approximately proportional to the volume flow rate of supply air. The relationship between the volume flow rate of supply air and its energy consumption can be fitted with a third-order polynomial as shown below [53]:

$$P_{ven} = \omega V_c^3, \tag{16}$$

where ω is a coefficient that can be assumed to be constant.

In this study, the coefficients of the models (13)-(15) are obtained by the regression technique. The relative error (RE), the root mean square error (RMSE) and the coefficient of variance (CV) are used to assess the fitness of the regression models. In this research, experimental data is taken from [51], and the RE, RMSE and CV are 13.43%, 7.16% and 12.89%, respectively.

For open loop optimal control, the system is assumed to be in its steady state with the reference temperature, moisture content and CO_2 concentration maintained. Therefore, let $T_{cs,ref}$, $W_{cs,ref}$ and $C_{c,ref}$ be the setpoints of air temperature, moisture content and CO_2 concentration in the conditioning room, respectively. The values of temperature and humidity setpoint are selected based on thermal comfort index. The value of CO_2 concentration setpoint is selected based on the requirements of occupants. Thermal comfort can be identified by a comfort zone within a psychometric chart [54]. The ASHRAE comfort zone is shown in Fig. 3. Let $T_{cs,ref}$ and $W_{cs,ref}$ be the two indicators selected from the comfort zone in Fig. 3. A steady state of the system (11) is such that

$$\begin{aligned}
&D^{-1}f_1(x, u) + D^{-1}f_2(z) = 0,\\
&T_{cs} = T_{cs,ref},\\
&W_{cs} = W_{cs,ref},\\
&C_c = C_{c,ref}.
\end{aligned} \tag{17}$$

To minimise the energy consumption of the DX A/C system, the objective function (12) is minimised while maintaining the value of indoor temperature, moisture content and CO_2 concentration in search of the steady state of the DX A/C system. For convenience, let x_i, $i = 1, 2, \ldots, 7$, denote each element of x, and let u_i, $i = 1, 2, 3$, denote each element of u. x and u should satisfy:

(C1) $T_{cs} \in [\underline{T}_{cs}, \overline{T}_{cs}]$, $W_{cs} \in [\underline{W}_{cs}, \overline{W}_{cs}]$. The air temperature and moisture content are within the comfort bounds. Comfort bounds $\underline{T}_{cs}, \overline{T}_{cs}, \underline{W}_{cs}$ and $\overline{W}_{cs}$ are design parameters, which are selected based on the comfort zone in Fig. 3.
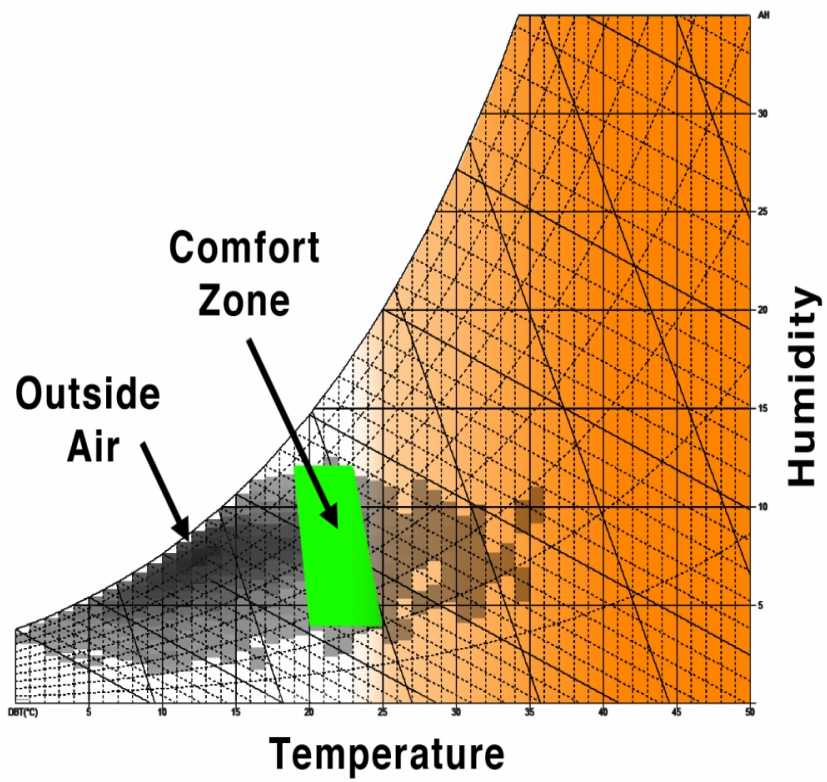
11

Figure 3: ASHRAE comfort zone representation.

(C2) $C_c \in [\underline{C}_c, \overline{C}_c]$ is the acceptable range of CO_2 concentration for occupants in the air conditioned room.

(C3) $T_e \in [\underline{T}_e, \overline{T}_e]$, $W_e \in [\underline{W}_e, \overline{W}_e]$. The supply air temperature and moisture content are limited by the air cooling coils and the physical characteristics of the coils. In addition, it is considered that the DX A/C is operating in the cooling mode, the bounds $\overline{T}_e$ and $\overline{W}_e$ are less than T_{cs} and W_{cs}, respectively.

(C4) $T_d \leq T_{cs}$, $T_w \leq T_{cs}$. The air temperature across the cooling coil can only decrease.

(C5) $V_f \in [\underline{V}_f, \overline{V}_f]$, $M_{rmf} \in [\underline{M}_{rmf}, \overline{M}_{rmf}]$, $V_c \in [\underline{V}_c, \overline{V}_c]$. These denote the allowed air volumetric flow rate, mass flow rate for refrigerant and volume flow rate of supply air. The lower bounds $\underline{V}_f$, $\underline{M}_{rmf}$ and $\underline{V}_c$ are strictly positive to meet minimum ventilation and operation requirements.

Thus, optimal scheduling is a nonlinear programming (NLP) problem with the objective function (12), equality constraints (17) and inequality constraints in (C3)-(C5). Therefore an optimisation problem is formulated as follows:

$$\min P_{total} \tag{18}$$

subject to:

$$D^{-1}f_1(x, u) + D^{-1}f_2(z) = 0,$$
$$T_{cs} = T_{cs,ref},$$
$$W_{cs} = W_{cs,ref},$$
$$C_c = C_{c,ref},$$
$$\underline{T}_e \leq T_e \leq \overline{T}_e,$$
$$\underline{T}_d \leq T_d \leq \overline{T}_d,$$
$$\underline{T}_w \leq T_w \leq \overline{T}_w,$$
$$\overline{W}_e \leq W_e \leq \overline{W}_e,$$
$$\underline{V}_f \leq V_f \leq \overline{V}_f,$$
$$\underline{M}_{rmf} \leq M_{rmf} \leq \overline{M}_{rmf},$$
$$\underline{V}_c \leq V_c \leq \overline{V}_c.$$

Let $T_{e,s}$, $T_{cs,ref}$, $T_{d,s}$, $T_{w,s}$, $W_{e,s}$, $W_{cs,ref}$, $C_{c,ref}$ and $V_{f,s}$, $M_{rmf,s}$, V_c denote the optimal solution to (18).

Remark 1: Eqs. (17) have many solutions as steady states. A specific operating point can be chosen for system analysis and controller design as was done in [40, 41]. In [55], the nonlinear building model was linearised around an equilibrium point which was obtained by fixing the input and then solving for the state point. Our proposal is an optimised open loop controller to steer the system to a setpoint which minimises an energy consumption model.

3.2. Linearisation for closed-loop controller

Define $\delta T_{cs} = T_{cs} - T_{cs,ref}$, $\delta W_{cs} = W_{cs} - W_{cs,ref}$, $\delta C_c = C_c - C_{c,ref}$, $\delta T_e = T_e - T_{e,s}$, $\delta T_d = T_d - T_{d,s}$, $\delta T_w = T_w - T_{w,s}$, $\delta W_e = W_e - W_{e,s}$, $\delta V_f = V_f - V_{f,s}$, $\delta M_{rmf} = M_{rmf} - M_{rmf,s}$ and $\delta V_c = V_c - V_{c,s}$ as the derivations of states and inputs from their steady states. Denote $x_0 \triangleq [T_{e,s}\ T_{cs,ref}\ T_{d,s}\ T_{w,s}\ W_{e,s}\ W_{cs,ref}$ $C_{c,ref}]^T$ and $u_0 \triangleq [V_{f,s}\ M_{rmf,s}\ V_{c,s}]^T$ as the steady state point of states and inputs, respectively. Therefore, the dynamic mathematical equation of DX A/C system can be linearised and written in a linear state-space representation:

$$\begin{cases} \delta \dot{x} = A_c(x_0, u_0)\delta x + B_c(x_0, u_0)\delta u, \\ y = C(\delta x + x_0), \end{cases} \tag{19}$$

where $\delta x \triangleq [\delta T_e\ \delta T_{cs}\ \delta T_d\ \delta T_w\ \delta W_e\ \delta W_{cs}\ \delta C_c]^T$ denotes the state deviation of the vector x from the steady state x_0, $\delta u \triangleq [\delta V_f\ \delta M_{rmf}\ \delta V_c]^T$ represents the input deviation of the vector u from the steady state u_0. $y \triangleq [T_{cs}\ W_{cs}\ C_c]^T$ are the original output variables. The coefficient matrices $A_c(x_0, u_0), B_c(x_0, u_0)$ can be calculated as follows:

$$A_c(x_0, u_0) = \left. \frac{\partial f(x, u)}{\partial x} \right|_{x=x_0, u=u_0}, \quad B_c(x_0, u_0) = \left. \frac{\partial f(x, u)}{\partial u} \right|_{x=x_0, u=u_0},$$

and the output matrix is:

$$C = \begin{bmatrix} 0 & 1 & 0 & 0 & 0 & 0 & 0 \\ 0 & 0 & 0 & 0 & 0 & 1 & 0 \\ 0 & 0 & 0 & 0 & 0 & 0 & 1 \end{bmatrix}.$$

Remark 2: The first order approximation of the Taylor based linearization is a classical method in control systems. It is locally valid in a neighborhood of the steady state. The loss of accuracy of linearization depends on the size of the local neighborhood, and is normally compensated by a closed-loop control for the transient to reach the steady state which is regulated by the open loop controller. Our closed-loop control is the MPC as proposed in the next section.

4. Model predictive control (MPC)

4.1. Discrete-time model

Consider the discrete-time version of (19):

$$\begin{cases} \delta x(k+1) = A_d(x_0, u_0)\delta x(k) + B_d(x_0, u_0)\delta u(k), \\ y(k) = C(\delta x(k) + x_0), \end{cases} \tag{20}$$

where k is the sampling instant; $x(k)$, $u(k)$ and $y(k)$ are the state vector, input vector and output vector at sampling instant k. $A_d(x_0, u_0) = e^{A_c(x_0, u_0)T_s}$, $B_d(x_0, u_0) = (\int_0^{T_s} e^{A_c(x_0, u_0)t} dt) B_c(x_0, u_0)$ are the system state matrix and input matrix, respectively. T_s is the sampling period.

14

4.2. Objective function

The objective of the proposed MPC controller is to maintain the comfortable indoor air temperature, moisture content and CO_2 concentration with low energy consumption. To this aim, the cost function to be minimised can be chosen as

$$\min_{\delta u} J = \min_{\delta u} (J_1 + J_2 + J_3 + J_4), \tag{21}$$

where

1. $\min J_1 = \min \sum_{i=1}^{N_p}(y_1(k+i) - T_{cs,ref}(k))^2$, which penalises that the comfortable indoor air temperature should be maintained;
2. $\min J_2 = \min \sum_{i=1}^{N_p}(y_2(k+i) - W_{cs,ref}(k))^2$, which indicates that the comfortable indoor air moisture content should be maintained;
3. $\min J_3 = \min \sum_{i=1}^{N_p}(y_3(k+i) - C_{c,ref}(k))^2$, which implies that the comfortable indoor air quality should be maintained;
4. $J_4 = \sum_{i=0}^{N_c-1} \|\delta u(k+i)\|_{\overline{R}}$, which reflects the consideration given to the size of u when the objective function J is made to be as small as possible.

Here, $\overline{R}$ is a diagonal matrix in the form that $\overline{R} = r_w I_{3N_c \times 3N_c}$ $(r_w > 0)$, where r_w is used as a tuning parameter for the desired closed-loop performance, and I is the identity matrix.

In the above objective functions, $y_1(k)$, $y_2(k)$, $y_3(k)$ are the kth step predicted temperature, moisture contents and CO_2 concentration, respectively. Define $Y = [y_1(k+1|k)\ y_2(k+1|k)\ y_3(k+1|k)\ \ldots\ y_1(k+N_p|k)\ y_2(k+N_p|k)\ y_3(k+N_p|k)]^T$, where $y_1(k+i|k)$, $y_2(k+i|k)$ and $y_3(k+i|k)$ denote the predicted value of $y_1(k)$, $y_2(k)$ and $y_3(k)$ at step i $(i = 1, \ldots, N_p)$ from sampling instant k. Define the reference vector $R_s = \overbrace{[I_{3\times 3}\ \ldots\ I_{3\times 3}]}^{N_p}{}^T r(k)$, where $[T_{cs,ref}(k)\ W_{cs,ref}(k)\ C_{c,ref}(k)]^T \triangleq r(k)$ are kth step setpoints temperature, moisture contents and CO_2 concentration. Define the predictive input variable $U = \left[\delta u^T(k)\ \delta u^T(k+1|k)\ \ldots\ \delta u^T(k+N_c-1|k)\right]^T$. N_p is the prediction horizon, N_c is the control horizon.

4.3. Constraints

The constraints of the control signal, the states can be introduced into the minimisation of the objective function (21). The constraints are described in (C1)-(C5). The optimisation problem to minimise the objective function (21) is a quadratic programming (QP) problem, which is a convex problem under the linear constraints condition.

4.4. MPC algorithm

With the help of the state space model (20), the objective function (21), and the constraints in (C1)-(C5), a general MPC algorithm is then applied to the DX A/C system. The procedure is designed as follows:

i. Calculate MPC gain matrices:

$$F = \begin{bmatrix} CA & (CA^2 & \ldots & CA^{N_p} \end{bmatrix}^T, \; M = \overbrace{\begin{bmatrix} C & C & \ldots & C \end{bmatrix}}^{N_p}{}^T,$$

$$\Phi = \begin{bmatrix} CB & 0 & \ldots & 0 \\ CAB & CB & \ldots & 0 \\ \vdots & \vdots & \ddots & 0 \\ CA^{N_p-1}B & CA^{N_p-2}B & \ldots & CA^{N_p-N_c}B \end{bmatrix}.$$

$E = \Phi^T\Phi + \overline{R}$, and $H = (F\delta x(k) + Mx_0 - R_s)^T\Phi$.

ii. According to MPC design, the predictive output vector can be expressed for input series: $Y = Mx_0 + F\delta x(k) + \Phi U$, and optimising the cost function can be written as:

$$\begin{aligned} & \min J \\ = \; & \min[(Y - R_s)^T(Y - R_s) + U^T\overline{R}U] \\ \Rightarrow \; & \min(U^T EU + 2HU). \end{aligned} \tag{22}$$

iii. Optimisation: find optimal U, such that the objective function given by (22) is minimised, and constraints in (C1)-(C5) are satisfied:

$$U^* = \arg\min_U \; (U^T EU + 2HU), \; \text{s.t. (C1)} - \text{(C5) hold.}$$

iv. Calculate the receding horizon control:

$$u^*(k) = [I_{3\times3}, 0, \ldots, 0]U^*.$$

v. Apply $u^*(k)$ to the system (20).

vi. Update time $k = k + 1$, and update system states, inputs and outputs with the control $u^*(k)$ and state equation (20). Repeat steps i to vi until k reaches its predefined value.

4.5. Features of the proposed MPC

In this paper, the focus is on the energy-efficient open loop optimiser and the closed-loop MPC. The overall steps of the proposed approach different from previous studies can be simply illustrated by Fig. 4. The more detailed structure of the proposed MIMO MPC with open loop optimisation is shown in Fig. 5. This figure describes the primary process of controlling the indoor air temperature, moisture content and CO_2 concentration, and open loop optimising energy consumption.

Different situations are simulated in the next section to illustrate the performances of the proposed strategy. In the first case, the proposed MPC control performances under different situations are discussed in the next section. In the second case, comparison of energy consumption for the proposed closed-loop MPC with different operating points under the same comfort conditions is studied in the next section. The more detailed analysis will be given after the simulation results.
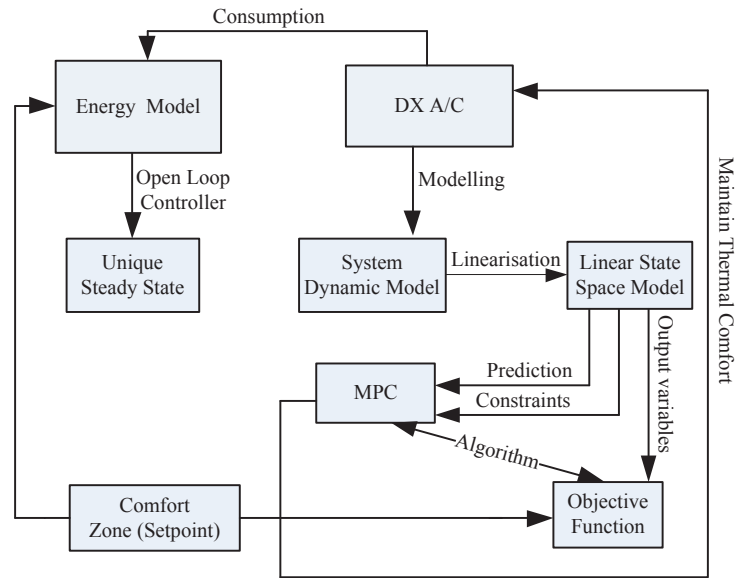
16

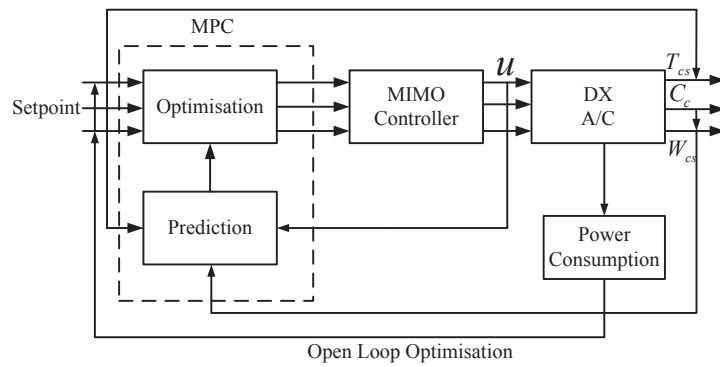Figure 4: Simplified flowchart of the proposed method.

Figure 5: Schematic diagram of the MIMO MPC with optimal control system.

5. Results and discussions

In this section, the proposed dynamic DX A/C model and control method are tested through simulation in a Matlab environment. Experimental data in [51] presented in Table 1 are used to justify the validity of the energy consumption model of the DX A/C system. The single-zone building as shown by Fig. 2 is used as the conditioning room in this paper. The model parameters of the DX A/C system given in Table 2 are adopted and validated in [40]. For the MPC strategy with open-loop optimisation, values of system constraints are listed in Table 3. The original nonlinear model (11) is used as the plant to be controlled in the simulation.

Table 1: Coefficients of the energy consumption models.

a_0=900.5	$a_1 = -8.1$	$a_2 = 6.18$	$a_3 = -0.15$	$a_4 = -4.61$
$a_5 = 0.02$	$a_6 = -0.2$	$a_7 = 0.01$	$a_8 = 0.12$	$a_9 = 0.09$
$b_0 = -1720$	$b_1 = 82$	$b_2 = -0.7$	$b_3 = 2.4$	$b_4 = -2.5$
$b_5 = 2.68$	$b_6 = 0.03$	$b_7 = -0.02$	$b_8 = 0.04$	$b_9 = 0.0001$
$c_0 = 138.1$	$c_1 = 0.52$	$c_2 = -2.3$		

Table 2: Numerical values of the system parameters.

Notations	Values	Notations	Values
C_a	1.005 kJ kg^{-1} °C^{-1}	A_1	4.414 m^2
ρ	1.2 kg/m^3	A_2	17.656 m^2
h_{fg}	2450 kJ/kg	V_{h1}	0.04 m^3
V	77 m^3	V_{h2}	0.16 m^3
α_1	0.089 kW m^{-2} °C^{-1}	α_2	0.103 kW m^{-2} °C^{-1}
k_{spl}	0.0251 kJ/m^3	k_{fan}	0.0085 m^3/r
G	5.6×10^{-6} m^3/s		

5.1. MPC with open loop optimisation

For the MIMO MPC, its control performances are evaluated based on the following issues:

(1) Setpoint regulation.
(2) Reference following.
(3) Setpoint regulation in existence of load disturbances.

5.1.1. Setpoint regulation

Simulation cases of $p = 25\%$ exhausted air volume are investigated in this subsection. For this simulation, the indoor air temperature, moisture content and CO_2 concentration setpoints are selected as $T_{cs,ref} = 24$ °C, $W_{cs,ref} = 11.35/1000$ kg/kg and $C_{c,ref} = 780.5$ ppm, respectively.

Table 3: Values of system constraints.

Notations	Values	Notations	Values
$\overline{T}_{cs}$	26 °C	$\underline{T}_{cs}$	22 °C
$\overline{W}_{cs}$	12.3/1000 kg/kg dry air	$\underline{W}_{cs}$	10.4/1000 kg/kg dry air
$\overline{C}_c$	850 ppm	$\underline{C}_c$	750 ppm
$\overline{T}_e$	24 °C	$\underline{T}_e$	0 °C
$\overline{W}_e$	11.35/1000 kg/kg dry air	$\underline{W}_e$	0 kg/kg dry air
$\overline{T}_d$	24 °C	$\underline{T}_d$	0 °C
$\overline{T}_w$	24 °C	$\underline{T}_w$	0 °C
$\overline{M}_{rmf}$	0.11 kg/s	$\underline{M}_{rmf}$	0 kg/s
$\overline{V}_f$	0.8 m³/s	$\underline{V}_f$	0 m³/s
$\overline{M}_{rmf}$	0.1 kg/s	$\underline{M}_{rmf}$	0 kg/s
$\overline{V}_c$	3 m³/s	$\underline{V}_c$	0 m³/s

In the case of 25% exhausted air volume and from Table 2, we follow the process as in (18), and the unique set of steady state is given in Table 4. The state matrix A_c and input matrix B_c of the corresponding system (19) are presented in Appendix A. To verify the closed-loop MPC performance, the following parameters are given. The prediction horizon N_p and control horizon N_c are set to 24 and 24, respectively. The tuning parameter $r_w = 0.5$ is set. The sampling interval is 2 minutes, and the total simulation time is $K = 24$ hours. To optimise the temperature, humidity and CO_2 concentration level, several types of constraints exist in the DX A/C system. To test the robustness of the closed-loop system, the disturbance vector is included in the simulation. The initial values of state variables are 23, 23, 23, 15, 12.44/1000, 13.5/1000 and 0.001, respectively. The initial values of input variables are 0.309, 0.0415 and 0.7, respectively. In addition, it is assumed the current indoor air temperature, moisture content and CO_2 concentration are 30 °C, 13.5/1000 kg/kg and 1000 ppm, respectively. The unit of relative humidity (RH) is percent (%). 11.35/1000 kg/kg moisture content is equivalent to 60% RH in conditioned space.

The performance of the proposed MPC is shown in Figs. 6-7. Fig. 6 depict simultaneous control of the indoor air temperature, relative humidity and CO_2 concentration in a conditioned space by the DX A/C system. It can be seen from Fig. 6 that, based on the proposed closed-loop MPC, the indoor air temperature, relative humidity and CO_2 concentration can reach their setpoints. As can be seen from Fig. 7, the MIMO controller corresponding to the setting indoor air temperature, humidity and CO_2 concentration level requires simultaneously varying the speed of the supply fan, compressor speed and volume flow rate of supply air for the DX A/C system. The setpoint is approached, and the indoor temperature, relative humidity and CO_2 concentration are maintained around the setpoint afterwards. It can be observed that with the proposed strategy, the indoor air temperature, relative humidity and CO_2 concentration of the closed-loop system are capable of reaching their setpoints of 24 °C, 60%

Table 4: Operating condition of the DX A/C system in the case of $p = 25\%$ exhausted air volume.

Parameter	Description or value	Parameter	Description or value
$T_{e,s}$	11.5 °C	$W_{e,s}$	8.665/1000 kg/kg dry air
$T_{cs,ref}$	24 °C	$W_{cs,ref}$	11.35/1000 kg/kg dry air
$T_{d,s}$	15 °C	$T_{w,s}$	12 °C
$M_{rmf,s}$	0.045 kg/s	$V_{f,s}$	0.298 m^3/s
$S_{fan,s}$	2102 rpm	$V_{sc,s}$	4243 rpm
$C_{c,ref}$	780.5 ppm	$V_{c,s}$	0.097 m^3/s
ν	3.665 kW	γ	1.396 kW
T_0	30 °C	W_0	13.5/1000 kg/kg dry air
C_0	300 ppm		

and 780.5 ppm after a transient process of 20 minutes. After reaching their setpoints, the variation ranges of indoor air temperature, relative humidity and CO_2 concentration are about ± 0.5 °C, $\pm 5\%$ and ± 9 ppm, respectively. Therefore the proposed MPC can effectively guarantee setpoint regulation of indoor air temperature, relative humidity and CO_2 concentration simultaneously by varying the compressor speed, supply fan speed and volume flow rate of the supply air of the DX A/C system.

5.1.2. Reference following capability test

In the reference following tests, it is expected that when the reference point changes, the MIMO MPC would react so that the new reference point can be maintained.

The initial reference points for indoor air temperature, moisture content and CO_2 concentration are selected as 24 °C, 11.35/1000 kg/kg and 780.5 ppm, respectively. After 12:00 pm, we change the reference points to 20.5 °C, 10/1000 kg/kg and 650 ppm, respectively. Thus, the steady state, variable constraints and system matrices are changed. The constraints of indoor air temperature, moisture content and CO_2 concentration are listed as follows: The constraints are from 18 °C to 22 °C, 9.5/1000 kg/kg to 11.5/1000 kg/kg and 600 ppm to 700 ppm, respectively. The open loop method is repeatedly used around the changing reference points to optimise the energy consumption model (12).

Figs. 8-9 illustrate the results of the proposed MIMO MPC with respect to the changing reference points of indoor air temperature, relative humidity and CO_2 concentration. When the reference indoor air temperature decreases from 24 °C to 20.5 °C, the reference of indoor air moisture content changes from 11.35/1000 kg/kg to 10/1000 kg/kg, and the reference of indoor air CO_2 concentration from 780.5 ppm to 650 ppm, the steady operation point of the DX A/C system's supply air temperature and moisture content have to be changed correspondingly from 11.5 °C to 10.4 °C and 8.665/1000 kg/kg to 7.5/1000 kg/kg, respectively. During the first 12 hours of the simulation, the
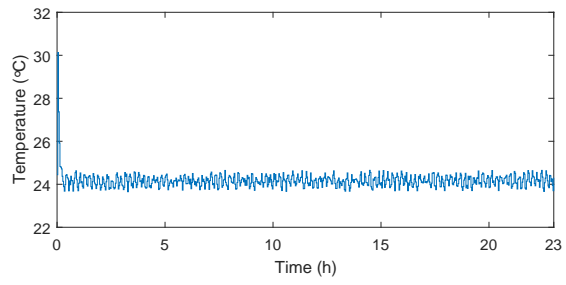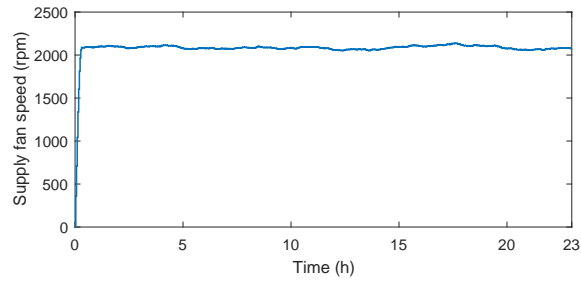
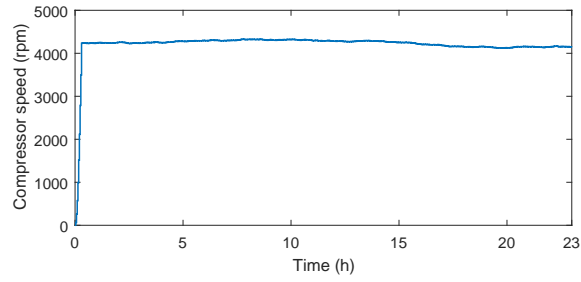(a) Indoor temperature
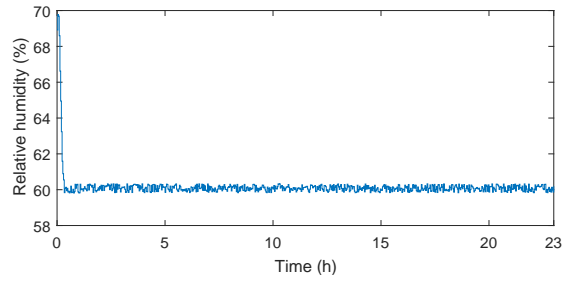
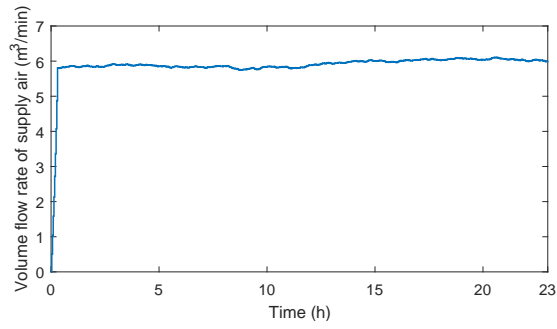(b) Indoor relative humidity
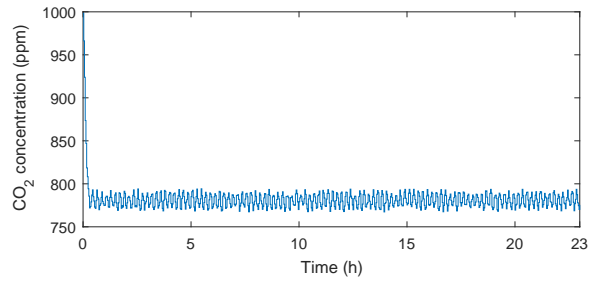
(c) Indoor CO_2 concentration

Figure 6: Setpoint regulation of indoor air temperature, relative humidity and CO_2 concentration in the case of 25% exhausted air volume.

(a) Supply fan speed

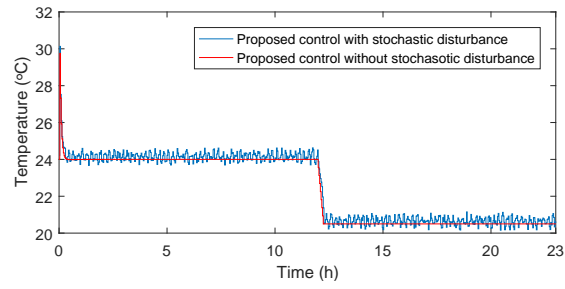(b) Compressor speed

(c) Volume flow rate of supply air

Figure 7: Profiles of supply fan speed, compressor speed and volume flow rate of supply air of the closed-loop system in the case of 25% exhausted air volume.

DX A/C system is stable, and the indoor air temperature, the moisture content and the CO_2 concentration are maintained at their corresponding reference points. At $t = 12$ hours, the change of indoor air temperature, moisture content and CO_2 concentration setting from 24 °C to 20.5 °C, 11.35/1000 kg/kg to 10/1000 kg/kg and 780.5 ppm to 650 ppm are introduced, then the indoor air temperature, relative humidity and CO_2 concentration can follow their reference changes immediately under the proposed MPC. The change of setpoint is reached after a transient process of 16 minutes. From Fig. 8, it can be seen that the MIMO MPC can well control the indoor air temperature, humidity and CO_2 concentration to its reference change.

It can be seen from Fig. 9, after the reference points of indoor air temperature, relative humidity and CO_2 concentration are changed, the steady operation points of the varying speed of the supply fan, the speed of the compressor and the volume flow rate of supply air have to be changed correspondingly from 2102 rpm to 2500.5 rpm, 4243 rpm to 5468.8 rpm and 5.8 m^3/min to 8.0 m^3/min, respectively. After reaching their setpoints, the variation ranges of indoor air temperature, relative humidity and CO_2 concentration are about ±0.5 °C, ±5% and ±9 ppm, respectively. Therefore, the test results shown in Figs. 8 and 9 suggest that the performance of the proposed MIMO MPC has in terms of the reference following capability.

### 5.1.3. Disturbance rejection capability test

The output variables, i.e., the indoor air temperature, the relative humidity and CO_2 concentration are to be maintained at their respective setpoints through simultaneously varying compressor speed, supply fan speed and volume flow rate of supply air when the space is subjected to disturbances of space sensible heat load, latent heat load and CO_2 emission load. Figs. 11-12 show the test results of disturbance rejection capability of the proposed MIMO MPC controller. The variation profile of sensible heat load, latent heat load and CO_2 emission loads imposed on the whole test period is shown in Fig. 10. The indoor air temperature, moisture content and CO_2 concentration constraints are listed as follows: The constraints are from 22 °C to 26 °C, 10.5/1000 kg/kg to 12.5/1000 kg/kg and 700 ppm to 850 ppm, respectively. At $t = 8$ h, the sensible heat load, latent heat load and CO_2 emission load increase from 4.8 kW to 5.376 kW, 1.397 kW to 1.607 kW and 46.4 m^3/s to 69.6 m^3/s, respectively, as shown in Fig. 10. Then, the operation points of the DX A/C control system are changed due to the increased disturbances. The variation profile of indoor air temperature, relative humidity and CO_2 concentration are shown in Fig. 11. During the first 8 hours of the test, the indoor air temperature, relative humidity and CO_2 concentration are maintained at 24 °C, 60% and 780.5 ppm, respectively, before the disturbance occurs. Afterward, the change of indoor air temperature, relative humidity and CO_2 concentration are slowly increased from 24.5 °C, 60% to 68% and 780.5 ppm to 791 ppm respectively, then the supply fan speed, compressor speed and volume flow rate of the supply fan are increasing to maintain the indoor air temperature, relative humidity and CO_2 concentration at their setpoints, as shown in Fig. 11 and Fig. 12. Fig. 12 presents
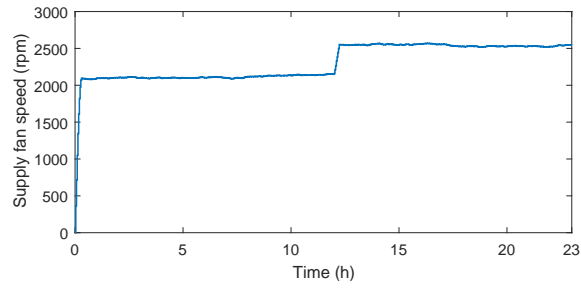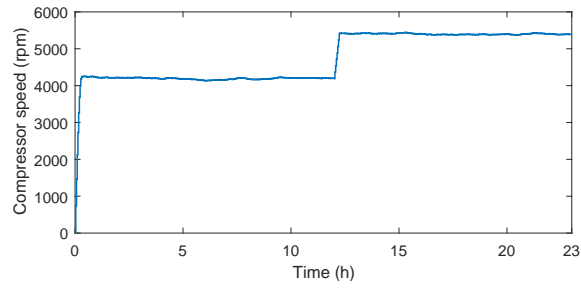
(a) Indoor temperature
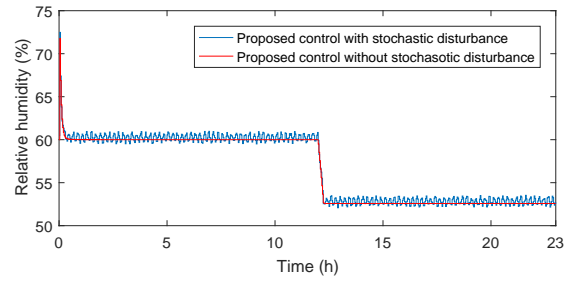
(b) Indoor relative humidity
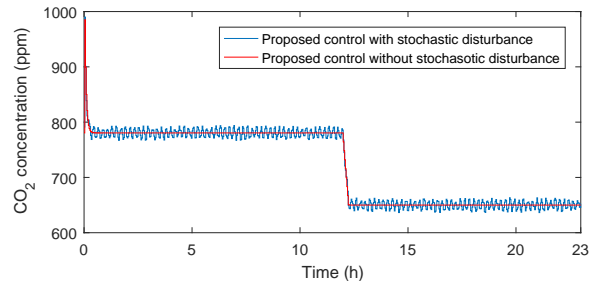
(c) Indoor CO_2 concentration

Figure 8: Reference following of indoor temperature, relative humidity and CO_2 concentration.
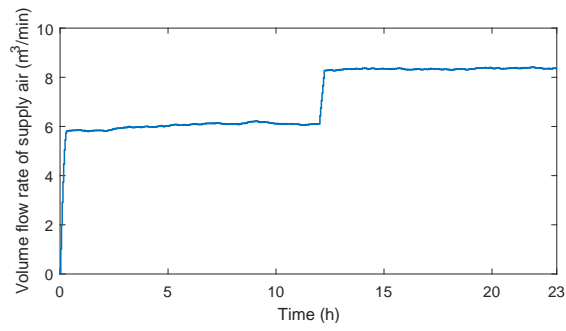
(a) Supply fan speed


(b) Compressor speed

(c) Volume flow rate of supply air

Figure 9: Supply fan speed, compressor speed and volume flow rate of supply air for closed-loop system based on reference following in the case of 25% exhausted air volume.

the variation profiles of the supply fan speed, compressor speed and volume flow rate of supply air. The supply fan speed, compressor speed and volume flow rate of supply air are increased simultaneously for maintaining indoor air temperature, relative humidity and CO_2 concentration at their setpoints. The stabilised operation points of the speed of supply fan, compressor speed and volume flow rate of supply air are around 2103 rpm, 4243 rpm and 5.82 m^3/s at the end of the test, respectively. It can be seen from Fig. 11, after reaching their setpoints, the variation ranges of indoor air temperature, relative humidity and CO_2 concentration are about ± 0.5 °C, $\pm 5\%$ and ± 9 ppm, respectively. Therefore, the proposed MIMO MPC controller can well control the indoor air temperature, relative humidity and CO_2 concentration to their respective setpoints, and in terms of disturbance rejection capability is satisfactory.
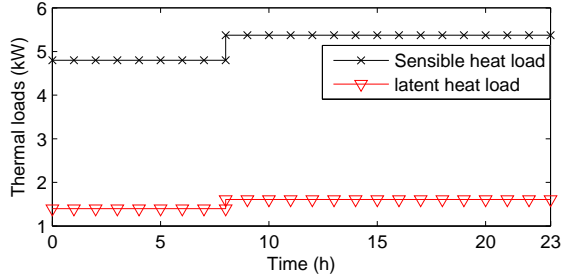


(a) Thermal loads
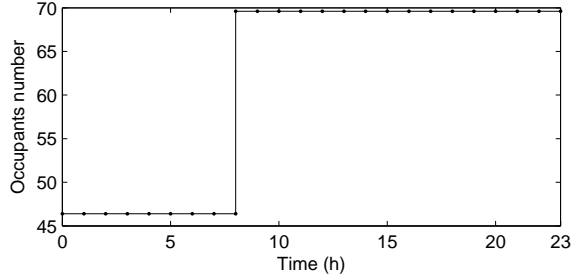
(b) CO_2 emission load

Figure 10: The variation profile of thermal and CO_2 emission loads of disturbance rejection capability test in the case of 25% exhausted air volume.

5.2. Analysis on energy saving

The control objective is to minimise energy q that is given by the formula $q = \sum_{k=0}^{T-1} P_{total}(k)t_s$, where T is total time; t_s is the sampling time; P_{total} is described in (12). In this paper, $T = 24$ hours and $t_s = 2$ minutes are selected. There are several ways to evaluate the performance of the different controllers. Comparisons are conducted in the following scenarios.
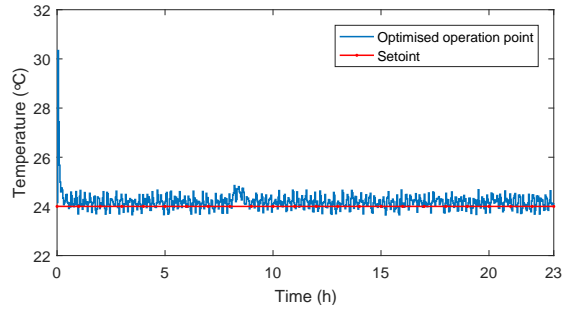
(a) Indoor temperature
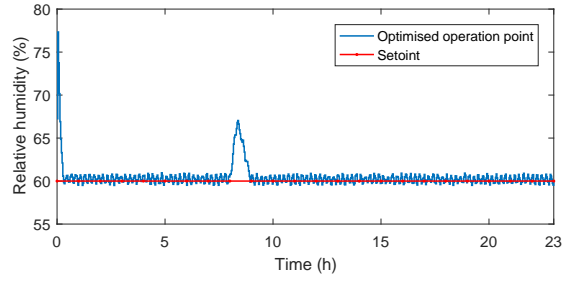
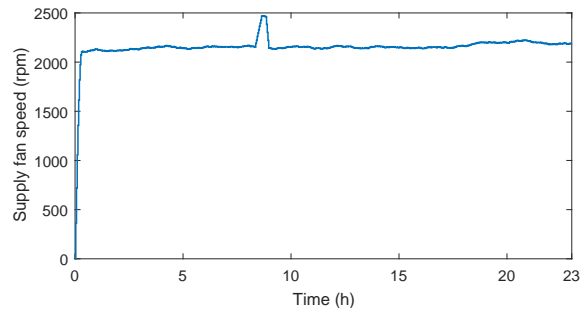
(b) Indoor relative humidity
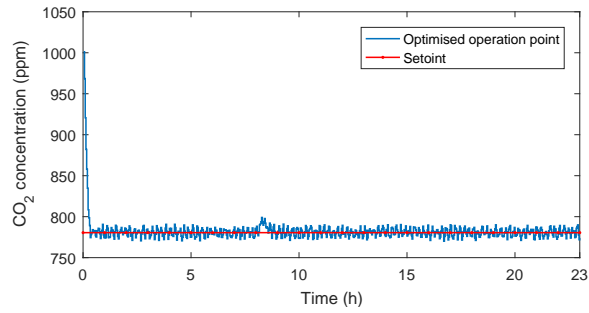
(c) Indoor CO_2 concentration

Figure 11: The variation profiles of indoor temperature, relative humidity and CO_2 concentration of disturbance rejection capability test in the case of 25% exhausted air volume.
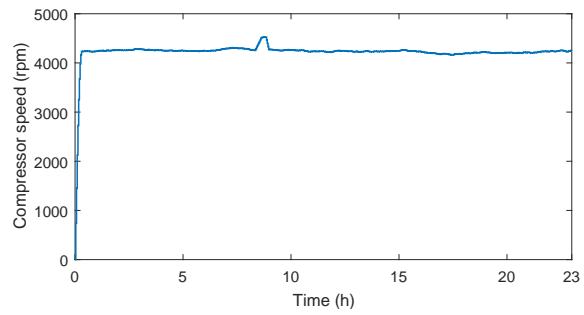
(a) Supply fan speed
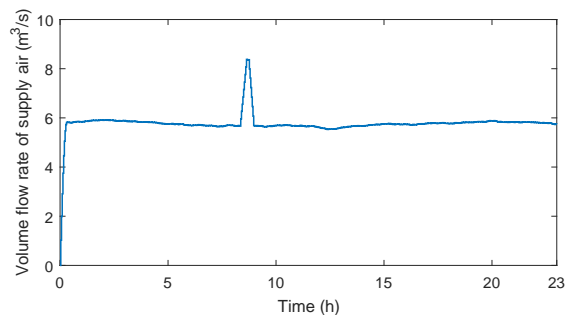
(b) Compressor speed

(c) Volume flow rate of supply air

Figure 12: The variation profiles of supply fan speed, compressor speed and volume flow rate of supply air of disturbance rejection capability test in the case of 25% exhausted air volume.

1) To illustrate the performance of the proposed MPC with energy-optimised open loop controller better, comparisons with other techniques are presented. The energy consumption of the DX A/C system with different techniques is indicated in Table 5. The MPC with a specific operation point strategy can be described as follows: The nonlinear DX A/C system is linearised around the specific operation point. The MPC controller is proposed to regulate the indoor air temperature, humidity and CO_2 concentration along the specific operation point. The MPC with a equilibrium point is described as below: The equilibrium point is obtained by fixing the speed of the compressor, speed of the supply fan and volume flow rate of the supply air, being 50% of their maximum values respectively, to solve the state point. Then the nonlinear DX A/C system is linearised around the equilibrium point. The MPC controller is presented to optimise the transient processes reaching the equilibrium point. It can be indicated by the results presented in Table 5 that the robustness of the proposed MPC is superior to that of the two strategies.

2) Energy consumption of the proposed energy-based open loop optimisation and closed-loop MPC in various situations is displayed in Table 6. The setpoint regulation strategy performs the best energy efficiency. It can be seen from Table 6 that, in the case of load disturbances, energy consumption increases, because of the necessity to remove more heat. The DX A/C system consumes more energy in the case of following reference change.

Table 5: Energy consumption of the closed-loop system for the proposed MPC control with different operation points.

Control strategy	Energy consumption (kWh/day)
Optimised operation point	17.26
Specific operation point	18.65
Equilibrium point by fixing the input	21.96

Table 6: Energy consumption of the closed-loop system with the proposed MPC in different situations.

Situation	Energy consumption (kWh/day)
Setpoint regulation	17.26
Reference change following	24.15
Setpoint regulation with load disturbances	19.64

6. Conclusions

In this paper, an MPC strategy is proposed to achieve optimal indoor temperature, humidity and CO_2 concentration simultaneously by varying speed of the compressor, varying speed of the supply fan and volume flow rate of supply

air for the DX A/C system in the perspective of energy-efficiency. The proposed MPC is designed based on open loop optimisation and closed-loop MIMO control. The main contributions of this research are four-fold: 1) by using open loop optimisation, the unique steady state of optimal indoor temperature, humidity and CO_2 concentration can be obtained; 2) the indoor air temperature, humidity and CO_2 concentration are maintained simultaneously by using the proposed MPC technique; 3) the couplings between indoor air temperature, humidity and CO_2 concentration are considered, whereas most other previous works studied energy efficiency in either temperature control or humidity control or CO_2 concentration control; and 4) as is supported by simulation results, energy efficiency has been improved while keeping optimal indoor temperature, humidity and CO_2 concentration.

It can be seen from both theoretical and simulation results that the closed-loop DX A/C system with the proposed MPC displays satisfactory performances and energy efficiency. As presented in simulation, the proposed MPC with optimising steady state can save 1.39 kWh/day more energy (compared with the proposed MPC with a specific operation point). The results of the proposed method show that CO_2 emissions can be reduced by 502.28 kg per annum (saving 1 kWh can reduce 0.99 kg CO_2 emissions[1]). The proposed MPC approach is reasonably effective for saving energy and CO_2 emissions.

The proposed energy-based optimised open loop controller and closed-loop regulation of MPC strategy is suitable for residential and office buildings using DX A/C system. For buildings using HVAC system, the proposed control method can be also modified to suit the need. Future works of this research may include a new approach that can be used to find the optimal time-varying reference of the DX A/C system to improve thermal comfort and energy efficiency.

Appendix A. System matrices

The system matrices for the DX A/C system are listed as follows:

---

[1]http://www.integratedreport.eskom.co.za/.

$$
A_c = \begin{bmatrix}
-2.8372 & 0 & -1.2297 & 4.0669 & -1959.2805 & 1469.4603 & 0 \\
0.0039 & -0.0039 & 0 & 0 & 0 & 0 & 11.3071 \\
0 & 4.3962 & -11.5218 & 8.1436 & 0 & 0 & 0 \\
0.0314 & 0.0051 & 0.0381 & -0.0763 & 0 & 0 & 0 \\
-0.0015 & 0 & -0.0007 & 0.0022 & -1.0588 & 0.7941 & 0 \\
0 & 0 & 0 & 0 & 0.0039 & -0.0039 & 0.0054 \\
0 & 0 & 0 & 0 & 0 & 0 & -0.0013
\end{bmatrix},
$$

$$
B_c = \begin{bmatrix}
30.6267 & 0 & 0 \\
-0.1621 & 0 & 0 \\
225 & 0 & 0 \\
0 & -4.2254 & 0 \\
0.0166 & 0 & 0 \\
-0.00003 & 0 & 0 \\
0 & 0 & -0.000006
\end{bmatrix}.
$$

References

[1] X. Xia, J. Zhang, Energy Efficiency and Control Systemsfrom a POET Perspective, IFAC Proceedings Volumes, 43 (2010) 255-260.

[2] X. Xia, J. Zhang, W. Cass, Energy management of commercial buildings-A case study from a POET perspective of energy efficiency, Journal of Energy in Southern Africa, 23 (2012) 23-31.

[3] H. Tazvinga, X. Xia, J. Zhang, Minimum cost solution of photo-voltaicdieselbattery hybrid power systems for remote consumers, Solar Energy, 96 (2013) 292-299.

[4] H. Tazvinga, B. Zhu, X. Xia, Energy dispatch strategy for a photo-voltaicwinddieselbattery hybrid power system, Solar Energy, 108 (2014) 412-420.

[5] Z. Wu, H. Tazvinga, X. Xia, Demand side management of photovoltaic-battery hybrid system, Applied Energy, 148 (2015) 294-304.

[6] H. Tazvinga, B. Zhu, X. Xia, Optimal power flow management for distribut-ed energy resources with batteries, Energy Conversion and Management, 102 (2015) 104-110.

[7] B. Zhu, H. Tazvinga, X. Xia, Switched model predictive control for energy dispatching of a photovoltaic-diesel-battery hybrid power system, IEEE Trans. on Control Systems Technology, 23 (2015) 1229-1236.

[8] Z. Wu, X. Xia, Optimal switching renewable energy system for demand side management, Solar Energy, 114 (2015) 278-288.

[9] E.M. Wanjiru, S.M. Sichilalu, X. Xia, Optimal control of heat pump water heater-instantaneous shower using integrated renewable-grid energy systems, Applied Energy (2016), Available: http://dx.doi.org/10.1016/j.apenergy.2016.10.041.

[10] A.J. Bijker, X. Xia, J. Zhang, Active power residential non-intrusive appliance load monitoring system, AFRICON 2009, 1-6.

[11] D. Setlhaolo, X. Xia, J. Zhang, Optimal scheduling of household appliances for demand response, Electric Power Systems Research, 116 (2014) 24-28.

[12] D. Setlhaolo, X. Xia, Optimal scheduling of household appliances with a battery storage system and coordination, Energy and Buildings, 94 (2015) 61-70.

[13] S.M. Sichilalu, X. Xia, Optimal power dispatch of a grid tied-battery-photovoltaic system supplying heat pump water heaters, Energy Conversion and Management, 102 (2015) 81-91.

[14] S.M. Sichilalu, X. Xia, Optimal energy control of grid tied PVdieselbattery hybrid system powering heat pump water heater, Solar Energy, 115 (2015) 243-254.

[15] D. Setlhaolo, X. Xia, Combined residential demand side management strategies with coordination and economic analysis, International Journal of Electrical Power and Energy Systems, 79 (2016) 150-160.

[16] E.M. Malatji, J. Zhang, X. Xia, A multiple objective optimisation model for building energy efficiency investment decision, Energy and Buildings, 61 (2013) 81-87.

[17] B. Wang, X. Xia, J. Zhang, A multi-objective optimization model for the life-cycle cost analysis and retrofitting planning of buildings, Energy and Buildings, 77 (2014) 227-235.

[18] B. Wang, X. Xia, Optimal maintenance planning for building energy efficiency retrofitting from optimization and control system perspectives, Energy and Buildings, 96 (2015) 299-308.

[19] Z. Wu, X. Xia, B. Wang, Improving building energy efficiency by multiobjective neighborhood field optimization, Energy and Buildings, 87 (2015) 45-56.

[20] B. Wang, Z. Wu, X. Xia, A multistate-based control system approach toward optimal maintenance planning, IEEE Transactions on Control Systems Technology, 25 (2017) 374-381.

[21] Z. Wu, B. Wang, X. Xia, Large-scale building energy efficiency retrofit: concept, model and control, Energy, 109 (2016) 456-465.

[22] Y. Fan, X. Xia, A multi-objective optimization model for energy-efficiency building envelope retrofitting plan with rooftop PV system installation and maintenance, Applied Energy, 189 (2017) 327-335.

[23] H. Carstens, X. Xia, X. Ye, Improvements to longitudinal Clean Development Mechanism sampling designs for lighting retrofit projects, Applied Energy, 126 (2014) 256-265.

[24] X. Ye, X. Xia, L. Zhang, B. Zhu, Optimal maintenance planning for sustainable energy efficiency lighting retrofit projects by a control system approach, Control Engineering Practice, 37 (2015) 1-10.

[25] E.M. Wanjiru, X. Xia, Energy-water optimization model incorporating rooftop water harvesting for lawn irrigation, Applied Energy, 160 (2015) 521-531.

[26] E.M. Wanjiru, L. Zhang, X. Xia, Model predictive control strategy of energy-water management in urban households, Applied Energy, 179 (2016) 821-831.

[27] N. Wang, J. Zhang, X. Xia, Energy consumption of air conditioners at different temperature set points, Energy and Buildings, 65 (2013) 412-418.

[28] J. Toftum, P.O. Fanger, Air humidity requirements for human comfort, ASHRAE Transactions, 105 (1999) 641-647.

[29] J.M. Hill, S.M. Jeter, Use of heat pipe exchangers for enhanced dehumidification, ASHRAE Transactions, 100 (1994) 91-102.

[30] D. Westphalen, K.W. Roth, J. Dieckmann, J. Brodrick, Improving latent performance, ASHRAE Transactions, 46 (2004) 73-75.

[31] A. Gasparella, G.A. Longo, R. Marra, Combination of ground source heat pumps with chemical dehumidification of air, Applied Thermal Engineering, 25 (2005) 295-308.

[32] A. Capozzoli, P. Mazzei, F. Minichiello, D. Palma, Hybrid HVAC systems with chemical dehumidification for supermarket applications, Applied Thermal Engineering, 26 (2006) 795-805.

[33] N. Wang, J. Zhang, X. Xia, Desiccant wheel thermal performance modeling for indoor humidity optimal control, Applied Energy, 112 (2013) 999-1005.

[34] R. Tu, X. Liu, Y. Jiang, Irreversible processes and performance improvement of desiccant wheel dehumidification and cooling systems using exergy, Applied Energy, 145 (2015) 331-344.

[35] G.Y. Yun, J. Choi, J.T. Kim, Energy performance of direct expansion air handling unit in office buildings, Energy and Buildings, 77 (2014) 425-431.

[36] Z. Li, S. Deng, An experimental study on the inherent operational characteristics of a direct expansion (DX) air conditioning (A/C) unit, Building and Environment, 42 (2007) 1-10.

[37] K.I. Krakow, S. Lin, Z.S. Zeng, Temperature and humidity control during cooling and dehumidifying by compressor and evaporator fan speed variation, ASHRAE Transactions, 101 (1995) 292-304.

[38] Z. Li, S. Deng, A DDC-based capacity controller of a direct expansion (DX) air conditioning (A/C) unit for simultaneous indoor air temperature and humidity control - Part I: control algorithms and preliminary controllability tests, International Journal of Refrigeration, 30 (2007) 113-123.

[39] Z. Li, S. Deng, A DDC-based capacity controller of a direct expansion (DX) air conditioning (A/C) unit for simultaneous indoor air temperature and humidity control-Part II: Further development of the controller to improve control sensitivity, International Journal of Refrigeration, 30 (2007) 124-133.

[40] Q. Qi, S. Deng, Multivariable control-oriented modeling of a direct expansion (DX) air conditioning (A/C) system, International Journal of Refrigeration, 31 (2008) 841-849.

[41] Q. Qi, S. Deng, Multivariable control of indoor air temperature and humidity in a direct expansion (DX) air conditioning (A/C) system, Building and Environment, 44 (2009) 1659-1667.

[42] N. Li, L. Xia, S. Deng, X. Xu, M. Chan, Dynamic modeling and control of a direct expansion air conditioning system using artificial neural network, Applied Energy, 91 (2012) 290-300.

[43] X. Xu, S. Deng, X. Han, X. Zhang, A novel hybrid steady-state model based controller for simultaneous indoor air temperature and humidity control, Energy and Buildings, 68 (2014) 593-602.

[44] Z. Li, X. Xu, S. Deng, D. Pan, A novel proportional-derivative (PD) law based fuzzy logic principles assisted controller for simultaneously controlling indoor temperature and humidity using a direct expansion (DX) air conditioning (A/C) system, International Journal of Refrigeration, 57 (2015) 239-256.

[45] Y. Zhu, X. Jin, X. Fang, Z. Du, Optimal control of combined air conditioning system with variable refrigerant flow and variable air volume for energy saving, International Journal of Refrigeration, 42 (2014) 14-25.

[46] Y. Zhu, X. Jin, Z. Du, X. Fang, B. Fan, Control and energy simulation of variable refrigerant flow air conditioning system combined with outdoor air processing unit, Applied Thermal Engineering, 64 (2014) 385-395.

[47] S.Y. Lin, S.C. Chiu, W.Y. Chen, Simple automatic supervisory control system for office building based on energy-saving decoupling indoor comfort control, Energy and Buildings, 86 (2015) 7-15.

[48] K. Gladyszewska-Fiedoruk, Correlations of air humidity and carbon dioxide concentration in the kindergarten, Energy and Buildings, 62 (2013) 45-50.

[49] R.Z. Freire, G.H.C. Oliveira, N. Mendes, Predictive controllers for thermal comfort optimization and energy savings, Energy and Buildings, 40 (2008) 1353-1365.

[50] S. Wang, X. Jin, Model-based optimal control of VAV air-conditioning system using genetic algorithm, Building and Environment, 35 (2000) 471-487.

[51] V. Vakiloroaya, B. Samali, K. Pishghadam, Investigation of energy-efficient strategy for direct expansion air-cooled air conditioning systems, Applied Thermal Engineering, 66 (2014) 84-93.

[52] ARI Standard 540, Performance Rating of Positive Displacement Refrigerant Compressors and Compressor Units, Air Conditioning and Refrigeration Institute, Arlington, VA, USA, 2004.

[53] G.P. Mehta, A. Thumann, Handbook of Energy Engineering, Lilburn, GA: Fairmont Press, 1989.

[54] ASHRAE, Handbook of Fundamentals, American Society of Heating, Refrigerating and Air Conditioning Engineers, Atlanta, GA, 2001.

[55] M. Maasoumy, Modeling and optimal control algorithm design for HVAC systems in energy efficient buildings, Master's thesis, EECS Depart., Univ. California, Berkeley, Feb. 2011. Available: http://www.eecs.berkeley.edu/Pubs/TechRpts/2011/EECS-2011-12.html.